Supplement of Geosci. Model Dev., 18, 3359–3385, 2025
https://doi.org/10.5194/gmd-18-3359-2025-supplement

Geoscientific Model Development
Open Access

Supplement of

UA-ICON with the NWP physics package (version ua-icon-2.1): mean state and variability of the middle atmosphere

Markus Kunze et al.

Correspondence to: Markus Kunze (kunze@iap-kborn.de)

Perpetual January simulations for tuning

This supplementary material documents the tuning process of the UA-ICON with the NWP physics package, which has led to the final decision of the parameters of the gravity wave parameterizations.

We perform a series of perpetual January simulations (Table S1) with variations of the scaling factor of the saturation momentum flux density (C^*) of WM96, introduced by McLandress and Scinocca (2005) when comparing H97, WM96, and Alexander and Dunkerton (1999) NGWD parameterizations. The total launch momentum flux in each azimuth ($\rho|\hat{F}_p|$) is tested

Label	C^*	$\rho_0\vert\hat{\mathbf{F}}_p\vert$	K_{wake}	K_{drag}	Fr_{crit}
NoOGWD	1.0	2.50	-	-	-
NoNGWD	-	-	1.5	0.075	0.4
NoGWD	-	-	-	-	-
F1C1 (NWPD)	**1.0**	**2.50**	**1.5**	**0.075**	**0.4**
F2C1	1.0	1.75	1.5	0.075	0.4
F2C10	10.0	1.75	1.5	0.075	0.4
F2C20	20.0	1.75	1.5	0.075	0.4
F2C30	30.0	1.75	1.5	0.075	0.4
F2C30-S (NWP)	**30.0**	**1.75**	**1.1**	**0.052**	**0.6**

Table S1. Parameter setting of the WM96 NGWD (C^*, $\rho_0|\hat{\mathbf{F}}_p|$) and the LM97 OGWD parameterizations of the tuning simulations in perpetual January mode; C^*, a factor to increase the saturation momentum flux density; $\rho_0|\hat{\mathbf{F}}_p|$, the total launch momentum flux in each azimuth in mPa; K_{wake}, the low-level wake drag constant; K_{drag}, the gravity wave drag constant; Fr_{crit}, the critical Froude number. All simulations use the same default settings for the WM96 tunable L_p = 450 hPa, the launch height of the gravity wave spectrum. The setups in bold are used for the UA-ICON(NWPD) and UA-ICON(NWP) simulations with a seasonal cycle.

with its default value of 2.50 mPa and compared with 1.75 mPa (setups labelled with F1 and F2, respectively), and the launch height (L_p = 450 hPa) stays with its default value. The simulation labelled with "-S" includes changes in tunable parameters of the OGWD parameterization, namely the low-level wake drag constant (K_{wake}), the gravity wave drag constant (K_{drag}), and the critical Froude number (Fr_{crit}).

Figure S1 shows profiles of averaged quantities for the Northern (NH) and Southern (SH) hemispheres, to evaluate the effect of parameter changes. By switching off the WM96 NGWD completely (NoNGWD), we can evaluate the effect of the parameterized NGWs. NoNGWD shows a strong response in the profiles for all averaged quantities, with the summer mesopause being too high in altitude and temperatures lower than the default (F1C1) case, but still too warm compared to SABER. The SH easterly wind regime extends to the lower thermosphere, and the meridional component of the residual MMC ($\overline{v}^*$) is even stronger northward directed than for F1C1, peaking near 100 km globally. The EP-flux divergence ($\nabla \cdot \mathbf{F}$) reflects the forcing of the zonal mean zonal wind by resolved waves. NoNGWD shows $\nabla \cdot \mathbf{F}$ more intense and in the opposite direction than F1C1, indicating an increase in dissipating resolved waves. These are probably GW with an eastward-directed phase speed, which can propagate to considerably higher altitudes in the easterly wind regime extending to the MLT region in the SH. For the simulation F2C1, the momentum flux $\rho|\hat{F}_p|$, launched near 450 hPa is decreased by 30%. With this, the zonal wind tendency due to NGWD decreases, and all other quantities slightly change in a direction discussed for NoNGWD, tending to worsen the climatology in the MLT. However, for simulations with an increasing C^* a smaller $\rho|\hat{F}_p|$ shows better results in the MLT. In the simulations, F2C10–F2C30, the parameterized WM96 NGWD increases by increasing the saturated momentum flux density from its default by a factor varying from $C^* = 10$ to $C^* = 30$, which effectively increases the altitude where the upward propagating NGWs dissipate with a direct impact on the tendency of the zonal wind in the MLT region calculated by the NGWD parameterization (NGWD). The weak eastward-directed NGWD of 40 m s^{-1} d^{-1} in the SH of the default (F1C1, Fig. S1) changes to 80 m s^{-1} d^{-1} (F2C10) or to more than 110 m s^{-1} d^{-1} (F2C20, F2C30, Fig. S1) within a shallow layer, peaking near 81 km. The magnitude of NGWD in F2C30 is comparable to NGWD of UA-ICON(ECHAM) (with the parametrization of Hines, 1997a, b, abbreviated as H97), which peaks slightly higher at 84 km and extends to a broader region in altitude. Near 100 km, NGWD changes to a westward direction in F2C20, F2C30, and in H97, with F2C20 and F2C30 showing a more narrow peak in NGWD than H97.

The summer mesopause temperature and the zonal wind regimes in the MLT region are changing, forced by the strengthened NGWD (Fig. S1). With increasing C*, the SH MLT temperature decreases in the simulations F2C10–F2C30, where the double peak structure of the mesopause in F1C1 and F2C1 is vanishing and only the lower part of the mesopause is persisting. The temperature is comparable to SABER but temperatures lower than 150 K concentrate in a narrow altitude region at $\sim$80–85 km, lower than SABER showing these temperatures between $\sim$84–93 km. The zonal wind direction reverses from the westward-directed summer circulation in the SH stratosphere/mesosphere to eastward zonal wind and from the eastward-directed winter circulation in the NH to westward zonal wind in the MLT. The NH polar cap mesopause temperature is increasing, a negative side effect, as the default settings (F1C1) already show a mesopause temperature slightly warmer than SABER. The temperature changes are directly related to changes in the MMC. As a measure of the strength of the MMC, we use $\overline{v}^*$ (Fig. S1), showing an increasing northward summer-to-winter directed flow with increasing C* in a layer around the mesopause. Above 100 km the MMC turns to a southward-directed flow with increasing C*, which is directly related to the more westward-directed NGWD-induced zonal wind changes in the SH and the change to an eastward-directed NGWD in the NH. This winter-to-summer directed flow extends over both hemispheres in a layer between 100 and 120 km with a minimum near the Equator, and is stronger in the NH for UA-ICON(NWP) than UA-ICON(ECHAM). Qian et al. (2017) and Wang et al. (2022) reported similar features for SD-WACCM simulations and compared them to the MMC derived from vertical gradients of SABER CO_2 volume mixing ratio. They found large vertical CO_2 gradients in the 95–110 km height region at summer hemispheric polar latitudes consistent with the SD-WACCM CO_2 gradients, and the upward-directed residual flow in the upper mesosphere and the downward-directed residual flow of the lower thermosphere.

Besides the average temperature, the variability and the range of temperatures in the summer mesopause region and the NH stratosphere are important measures. We use the probability density function (PDF) of daily January zonal mean temperature in selected areas near the NH stratopause, the NH lower stratosphere (Fig. S2), the SH mesopause, and stratopause (Fig. S3) to show the effect of GW parameter tuning of UA-ICON(NWP) in comparison to UA-ICON(ECHAM), SABER data, and ERA-5 reanalysis data. The temperature distribution near the stratopause (Fig. S2, a) confirms that all UA-ICON simulations are too warm, compared to SABER and ERA-5 when the non-orographic GW parametrization is on. The UA-ICON(NWP) simulations without NGWD parameterization (NoNGWD, NoGWD) show a slightly lower average temperature and a wider distribution than ERA-5. With the increasing strength of the NGWD, the NH stratopause temperatures increase, where all UA-ICON simulations with NGWD parameterization show a more narrow probability density function. In the NH lower stratosphere (Fig. S2, b) the average temperature is much too low without OGWD parameterization (NoOGWD) and even lower without any GW parameterizations (NoGWD). Most UA-ICON(NWP) simulations, with default settings (F1C1) and an increase (F2C10–F2C30) of the NGWD, show an average lower stratospheric temperature around 200 K, a cold bias of 4–8 K compared to ERA-5 and an even stronger cold bias compared to the $\sim$2 K higher temperature from SABER. The simulation F2C30-S, including adapted parameters for the OGWD parametrization, shows the best agreement with ERA-5 temperature which is only slightly colder, whereas UA-ICON(ECHAM) shows a warm bias and a narrow PDF, indicating a too-low inter-annual variability.

The temperatures in the SH mesopause region are the lowest in the Earth's atmosphere. The average SABER temperature is near 150 K with a range of temperatures from 110 to 180 K. Whereas UA-ICON(ECHAM) shows a cold bias in this region, the UA-ICON(NWP) simulations with default settings for the WM96 NGWD show a strong warm bias and the double peak structure of the mesopause temperature (Fig. S1) with a minimum near 90 km which also is reflected in the PDF, showing two distinct peaks. Decreasing $\rho|\hat{F}_p|$ by 30% (F2C1), slightly increases the temperatures, shifting the distribution towards the ones of NoNGWD and NoGWD, that, however, do not cover the region of the mesopause ($\sim$100–110 km) in these simulations and therefore show an average temperature slightly below 200 K. With increasing C* for the WM96 NGWD (F2C10–F2C30, F2C30-S) the average temperature decreases, and the range of temperature increases, where the lower tail of the PDF shows a two-peak structure comparable to UA-ICON(ECHAM). The SABER data show a Gaussian distribution and do not confirm the high temperatures of the upper tail of the PDF in the UA-ICON(NWP) simulations F2C30 and F2C30-S.

Derived from the numerical experiments, one parameter setup, F2C30-S, in Table S1 corresponding to C* = 30 and an adaptation of the OGWD parameters to values as indicated for F2C30-S, provides the most reasonable prediction and therefore is used for further investigations in the time slice simulation UA-ICON(NWP) discussed in the main text.

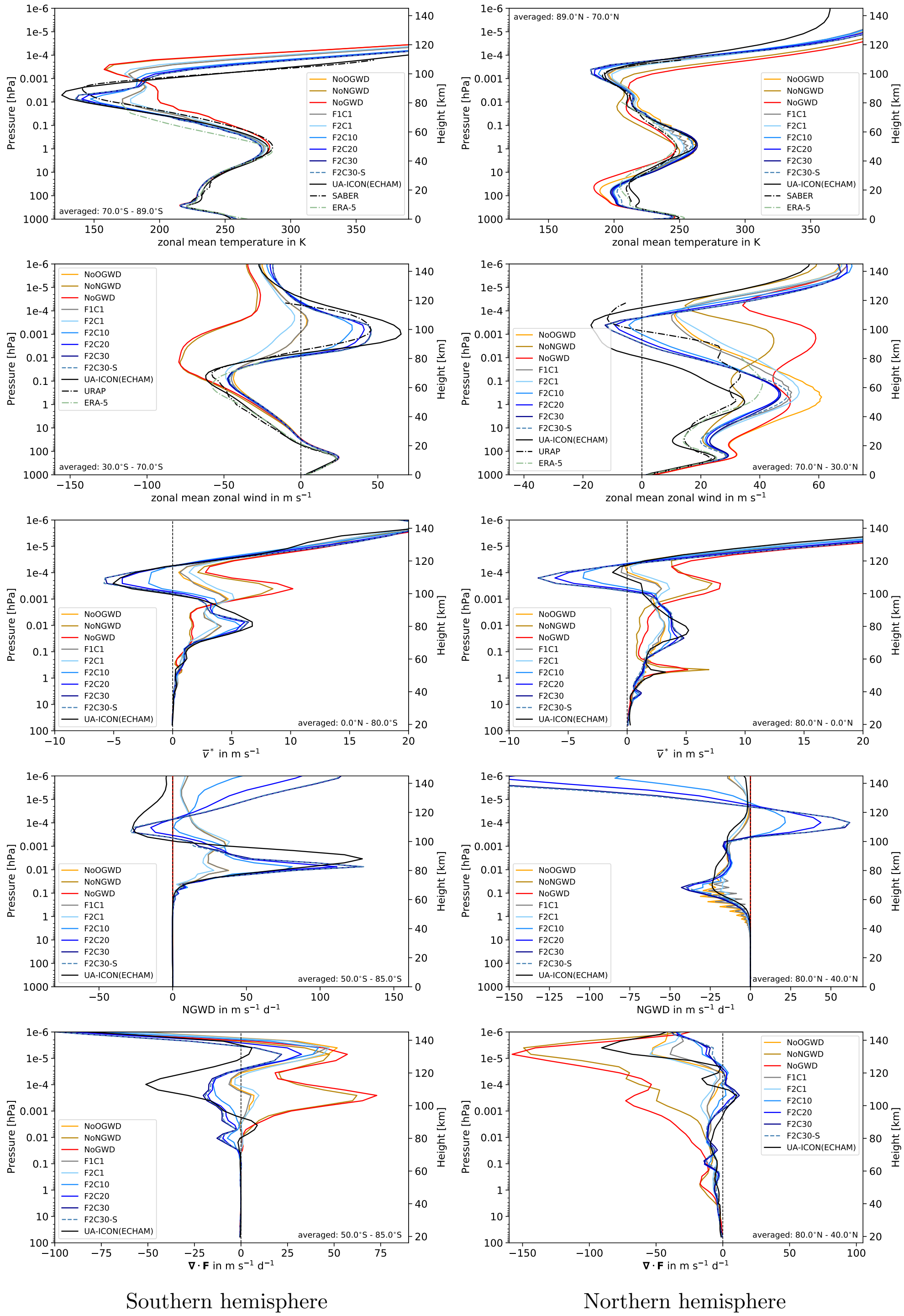

Figure S1. Vertical profiles of quantities averaged for specific regions in January for (left column) the Southern hemisphere; (right column) the Northern hemisphere; from top to bottom for the temperature in K; the zonal wind in m s^{-1}; the transformed Eulerian mean meridional velocity ($\overline{v}^*$) in m s^{-1}; the non-orographic gravity wave drag in m s^{-1} d^{-1}; and the divergence of the Eliassen-Palm vector ($\nabla \cdot \mathbf{F}$) in m s^{-1} d^{-1}.

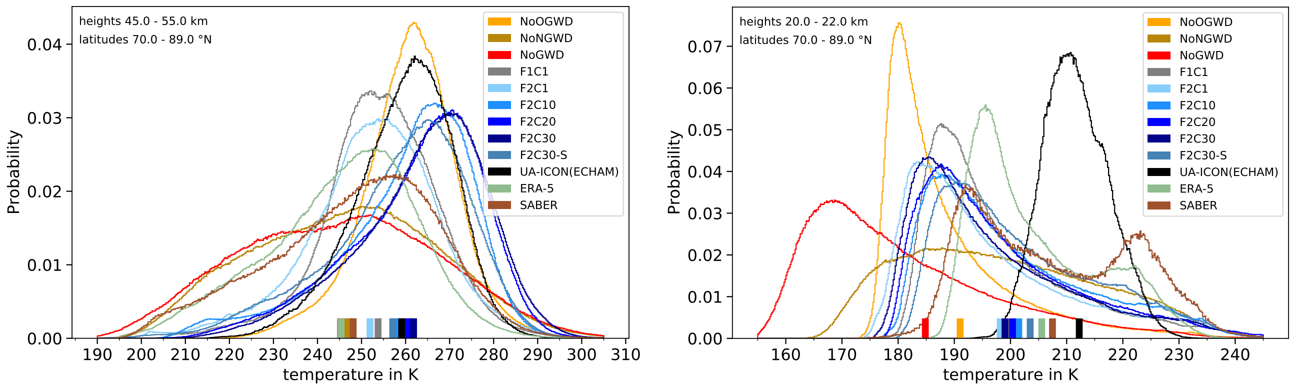

(a) NH stratopause (b) NH lower stratosphere

Figure S2. Probability density functions (PDF) of daily mean temperature, for ERA-5 and UA-ICON, and the original temperature soundings for SABER, in the northern hemisphere; (a) for the northern polar cap (70–89°N) stratopause region (45–55 km); (b) for the northern polar cap lower stratosphere (20–22 km).

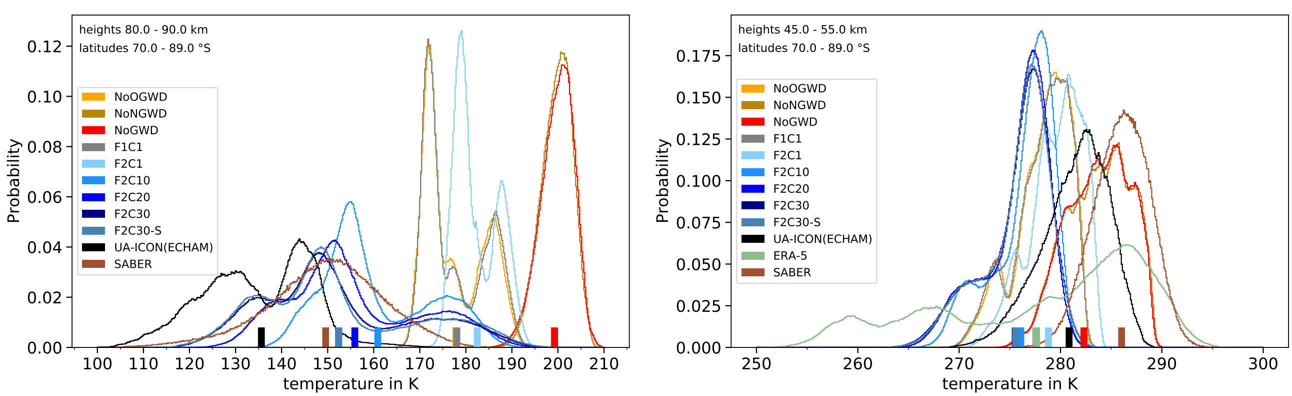

(a) SH mesopause (b) SH stratopause

Figure S3. As Figure S2; (a) for the southern polar cap (70–89°S) mesopause region (80–90 km); (b) for the southern polar cap stratopause (45–55 km).

Southern hemisphere springtime transition

The transition of the monthly mean zonal mean zonal wind from the wintertime westward-directed (easterly) flow to the summertime eastward-directed (westerly) flow in the SH is shown in Fig. S4. All data of the UA-ICON simulations is interpolated to constant pressure levels for this analysis. The transition to an easterly flow in 60 °S at 10-hPa occurs in early November for ERA-5 reanalysis data, which the UA-ICON(ECHAM) simulation matches perfectly. The UA-ICON(NWP) simulations show the transition in late November, which is only slightly shifted to a later date by the GWD tuning, compared with the WACCM experiments shown in Fig. 10 of Richter et al. (2010) which appear at the end of December.

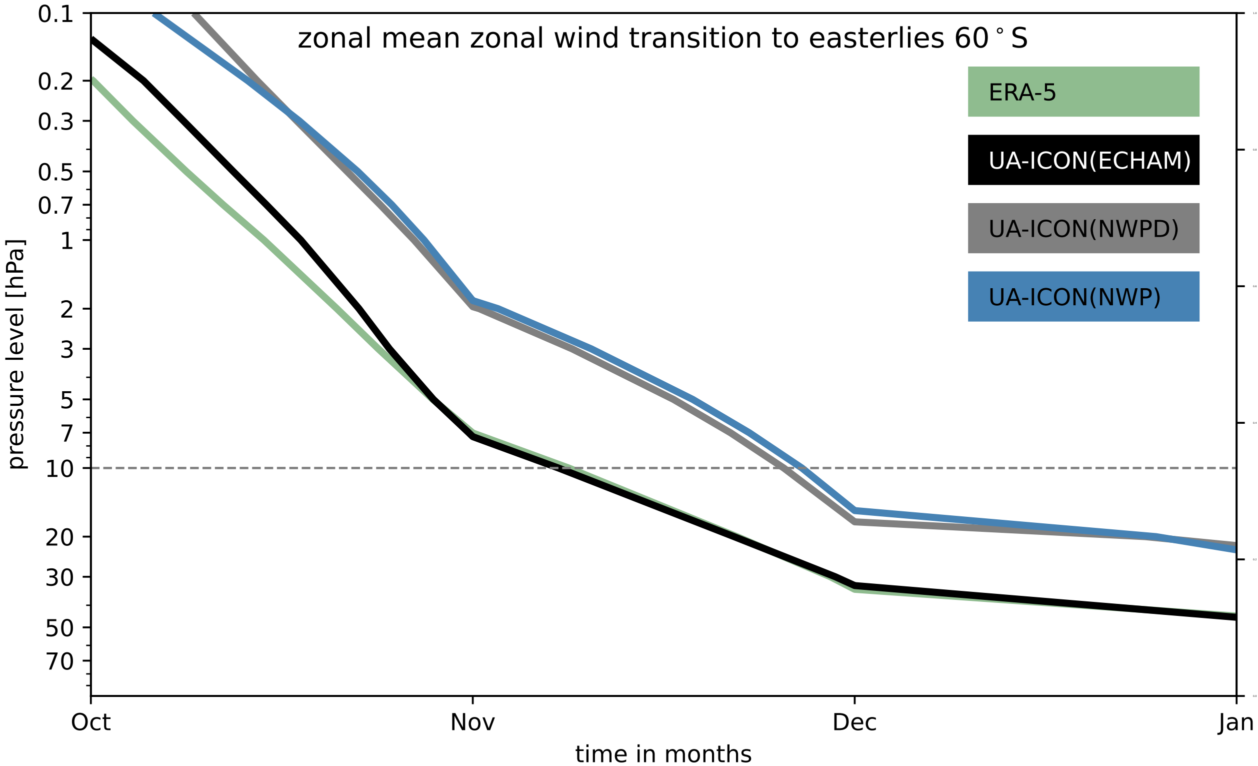

Figure S4. Time-pressure section at 60 °S of the zero zonal mean zonal wind contour for UA-ICON simulations and ERA-5 reanalysis.

References

Alexander, M. J. and Dunkerton, T. J.: A Spectral Parameterization of Mean-Flow Forcing due to Breaking Gravity Waves, J. Atmos. Sci., 56, 4167–4182, https://doi.org/10.1175/1520-0469(1999)056<4167:ASPOMF>2.0.CO;2, 1999.

Hines, C. O.: Doppler-spread parameterization of gravity-wave momentum deposition in the middle atmosphere. Part 1: Basic formulation, J. Atmosph. Solar-Terr. Phys., 59, 371–386, https://doi.org/10.1016/S1364-6826(96)00079-X, 1997a.

Hines, C. O.: Doppler-spread parameterization of gravity-wave momentum deposition in the middle atmosphere. Part 2: Broad and quasi monochromatic spectra, and implementation, J. Atmosph. Solar-Terr. Phys., 59, 387–400, https://doi.org/10.1016/S1364-6826(96)00080-6, 1997b.

McLandress, C. and Scinocca, J. F.: The GCM Response to Current Parameterizations of Nonorographic Gravity Wave Drag, J. Atmos. Sci., 62, 2394–2413, https://doi.org/10.1175/JAS3483.1, 2005.

Qian, L., Burns, A., and Yue, J.: Evidence of the Lower Thermospheric Winter-to-Summer Circulation From SABER CO 2 Observations, Geophys. Res. Lett., 44, 10,100–10,107, https://doi.org/10.1002/2017GL075643, 2017.

Richter, J. H., Sassi, F., and Garcia, R. R.: Toward a physically based gravity wave source parameterization in a general circulation model, J. Atmos. Sci., 67, 136–156, https://doi.org/10.1175/2009JAS3112.1, 2010.

Wang, N., Qian, L., Yue, J., Wang, W., Mlynczak, M. G., and Russell, J. M.: Climatology of Mesosphere and Lower Thermosphere Residual Circulations and Mesopause Height Derived From SABER Observations, J. Geophys. Res.: Atmos., 127, 1–14, https://doi.org/10.1029/2021jd035666, 2022.